FINITE ELEMENT MODELING, SIMULATION AND ANALYSIS OF COLD UPSETTING PROCESS OF DIE

Yaraguntla Pragathi[1,] Pedapudi AShok[2]
[1,2,]Assistant Professor in St Peter's Engineering College,
Mechanical Engineering Department, Hyderabad

Abstract

The basic idea in the finite element analysis (FEA) is to find the solution of a complicated problem by replacing it by a simpler one. Since a simpler one to find the solution replaces the actual problem, we will be able to find only an approximate solution rather than the exact solution [1]. The existing mathematical tools are not sufficient to find the exact solution of most of the practical problems. Thus in the absence of convenient method to find the approximate solution of 3-d problem, we have option for FEA. The FEA basically consists of the following procedure. First, a given physical or mathematical problem is modeled by dividing it into small interconnecting fundamental parts called Finite Elements. Next, analysis of the physics or mathematics of the problem is made on these elements: finally, the elements are re-assembled into the whole with the solution to the original problem obtained through this assembly procedure These approximating functions (also called interpolation model) are defined in terms of the values of the value of the field variable. By solving the field equations, which are generally in the form of matrix equations, the nodal value of the field variable will be known. Once these are known, the approximating functions define the field variable throughout the assemblage elements. The variations in FEA results compared to analytical results for AA 2024 alloy and AA2024 alloy- 2 - 10 % fly ash composites respectively. The obtained FEA results revealed that these values are closely matching with the experimental values with a maximum deviation of less than 5%. Hence the FEA model adopted for solving the present upsetting analysis was validated with the analytical results.

Index Terms: Fea, Friction analysis, Hyper Mesh.

I.INTRODUCTION

In the FEA, the actual continuum or the body of matter like solid, liquid or gas is represented as an assemblage of subdivisions called finite elements. The elements are considered to be interconnected at specified joints, which are called nodes or nodal points. The nodes usually lay on the element boundaries where adjacent elements are considered to be connected. Since, the actual variation of the field variable (like displacement, stress, temperature, pressure or velocity) inside the continuum is not known; we assume that by a simple function. These approximating functions (also called interpolation model) are defined in terms of the values of the value of the field variable. By solving the field equations, which are generally in the form of matrix equations, the nodal value of the field variable will be known. Once these are known, the approximating functions define the field variable throughout the assemblage elements

Many forming aspects can be analyzed from simulated solution. For instance, irregular flow, which can cause products internal defects, can be detected from simulation. Die filling problems can also be predicted by deformation pattern and stress/strain solutions. Elastic deformation of the tools, which should be controlled to maintain desirable tolerances, can be verified in the finite element analysis prediction. The solution convergence of the method is checked by decreasing the time step, and by increasing the number of nodes of the analysis model.

Computer simulation has become reliable and acceptable in the metal forming industry since the 1980's. Metal forming analysis can be performed in three modeling scales [2]. The first scale is the global modeling, which only predicts process loads or work. Analytical methods are used for this purpose. Local scale analysis is used to estimate the thermo-mechanical variables such as strain, strain rate, and temperature. With the extensive development in computational mechanics, numerical methods have been used as an economical alternative to perform the local modeling. Micro-scale modeling computes the micro-structural evolution during the forming process. Since global scale analysis is only applicable to simple situations and micro modeling is still incipient and only gives results for specific conditions, local modeling is the most popular approach. Among other methods, the Finite Element Methods (FEM) is widely used in metal forming analysis due to its capabilities to model the complicated geometries of tools and parts in forming processes

II.CONTACT ANALYSIS.

The contact problem is a kind of geometrically nonlinear problem that arises when different structures or different surfaces of a single structure, either come into contact or separate or slide on one another with friction. Contact forces, either gained or lost, must be determined in order to calculate structural behavior [3]. The location and extent of contact may not be known in advance, and must also be determined.

Contact algorithms in FM analysis allow contact elements to be attached to the surface of one of two FE discretization's that are expected to come in contact. A contact element is not a conventional finite element. Their functions is to sense contact and then supply a penalty stiffness or activate some other scheme for preventing or limiting interpenetration. Contact analysis is highly complex and nonlinear analysis. Contact problems fall into two general classes. One is rigid-to-flexible and flexible-to-flexible. In rigid-to-flexible contact problems, one or more of the contacting surfaces are treated as rigid, i.e., it has a much higher stiffness relative to the deformable body it contacts.

In general, any time a soft material comes in contact with hard material, the problem is assumed to be rigid-to-flexible, instances like: metal forming problems. The other class, flexible-to-flexible, is the more common type. In this case, both contacting bodies are deformable, i. e have similar stiffness. Example, bolted flanges. Ansys supports three contact models; node-to-node, node-to-surface and surface-to-surface contact. In problems involving contact between two boundaries, one of the boundaries is conventionally established as the target surface and the other as the contact surface. For rigid-flexible contact, the target surface is always the rigid surface and the contact surface is the deformable surface. For flexible-to-flexible contact, both surfaces are associated with deformable bodies. These two surfaces together comprise the contact pair. Ansys provides special elements for contact pair. Different contact elements are CONTAC12, CONTAC52, CONTAC 26, CONTAC 48, CONTAC 171,172, TARGET 169, CONTAC 173, and TARGET 170. Figure 1 shows the contact pair between die and composite model.

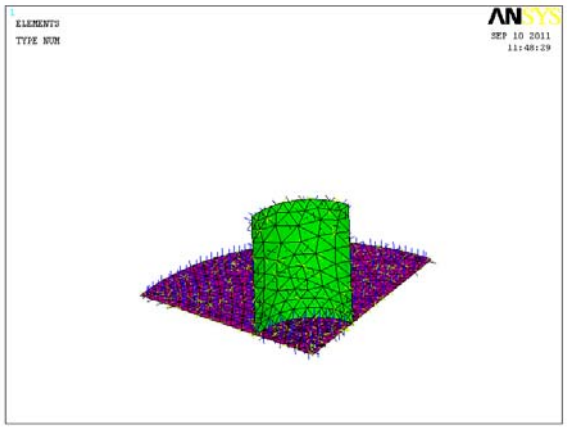

Fig 1: Contact pair between die and composite model

Material properties and real constants.

Steel has been chosen for die material. Its basic mechanical properties are Young's modulus E = 210 GPa and Poisson's Ratio = 0.29. The material properties of the underlying elements are used to calculate appropriate contact stiffness.

ANSYS estimates a default value for contact stiffness based on the material properties of the underlying deformable elements. In real constant set, Normal Contact Stiffness Factor (FKN) is used to specify either a scaling factor or an absolute value for contact stiffness. The scaling factors will usually

between 0.01 to10 a value of 1.0 (the default) is often a good starting value for bulk deformation problems, or 0.01-0.1 for bending dominated problems. FKN should always be verified in order to minimize penetration while avoiding excessive iterations.

In real constant set, Allowable maximum penetration factor (FTOLN) is a factor based on the thickness of the element, which specifies an allowable maximum penetration. If ANSYS detects any penetration larger than this tolerance, the global solution is still considered unconverged, even though the residual forces and displacements have met convergence criteria. The default for FTOLN is 0.1. Changing this value make the tolerance too small can cause an excessive number of iterations or non-convergence.

In real constant set, Initial closure factor (ICONT) is used to specify a small initial contact closure. This is the depth of an "adjustment band" around the target surface. A positive value for ICONT indicates a scaling factor relative to the depth of the underlying elements. A negative value indicates an absolute contact closure value.

A contact element is considered to be in near field contact when its contact element enters a pinball region, which is centered on the integration point of the contact element. Real constant Pinball region (PINB) can be used to specify a scaling factor (positive value for PINB) or absolute value (negative value for PINB) for pinball region. Table 1shows the overall material properties and real constants selected for solving the present problem:

TABLE 1: MATERIAL PROPERTIES AND REAL CONSTANTS

Normal Contact Stiffness Factor	FKN = 1.0
Allowable maximum penetration factor	FTOLN =0.1
Initial closure factor, (adjustment band)	ICONT =0.1
Pinball region	PINB =2.0

FRICTION IN METAL FORMING

Friction is the great importance in many metal forming operations. They affect the material flow, deformation characteristics of the work piece, wear and fatigue failure of the tool, and the mechanical properties of the formed parts. Furthermore, minimizing friction is profitable since it reduces the force and energy required for a given operation. This will lessen the stresses induced in the forming tool and prevent direct tool to work piece contact, which contribute to longer tool life and better quality control.

COMPRESSION TESTING OF SHORT CYLINDERS

The compression of a short cylinder between anvils is a much better test for measuring the flow stress in metal working applications [23-25]. The nature of tensile instability due to necking can be avoided and the test can be carried out to strains in excess of 2.0 (for ductile material). Friction between the specimen and anvils play key role. In the homogeneous upset (zero friction) test a cylinder of diameter D_0 and initial height H_0 would be compressed in height to H and spread out in diameter to D according to the law of constancy of volume.

$$D_0^2 H_0 = D^2 H$$

III. PROCEDURE ADOPTED IN MODELING THE PROBLEM UNDER TAKEN.

The computational modeling of each forming process stage by the finite element method can make the sequence design faster and more efficient, decreasing the use of conventional "trial and error" methods. In this study, the application of commercial general finite element software ANSYS 10.0 has been applied to model a forming operation. The basic data required for analysis of upsetting process are true stress- true strain behaviour and friction factor. The true stress- true strain data was obtained from upsetting test performed with frictionless (smooth surface finish) dies and aspect ratio of 1.0 on 100 kN UTM (Model: UT 9102; Dak system Inc). No lubricant was used during the test.

Finite element analysis of deformation behavior of cold upsetting process was carried out for the AA 2024 alloy and AA 2024 alloy - 2, 6 and 10 wt. % fly ash composites in dry condition with aspect ratios of 1.0 and 1.5. Due to axisymmetric nature of the geometry only quarter portion was modeled with symmetric boundary conditions. Rigid-flexible contact

analysis was performed for the forming process. The billet geometry was meshed with 10-node tetrahedral elements (solid 92 in ANSYS Library). The tetrahedral elements are more feasible in filling meshes into any complicated shape [4]. Element size was selected on the basis of convergence criteria and CPU time. Too coarse mesh may never converge and too fine mesh requires long CPU time without much improvement in accuracy.

The material models selected were based on the properties of the tooling and billet materials. Due to high structural rigidity of the tooling, only the following elastic properties of tooling (H13 steel) were assigned assuming the material to be isotropic [5].

Young's Modulus E = 220 GPa = 210 X 10^3 MPa

Poisson's ratio υ = 0.30

IV. Results and Discussions

Figure 2 and 3 shows the meshed models of billets and tooling for the aspect ratios of 1.0 and 1.5 respectively. Figure 4 and 5 shows the 50% deformation specimen with zero friction for the aspect ratios of 1.0 and 1.5 respectively. Since there was no friction at metal-die contact, the deformation can be treated as homogeneous since no bulging was seen. The maximum radial displacement corresponding to 50% for the aspect ratio of 1.0 is shown as 2.069 mm in figure 6. This means that the diameter after 50% deformation equals to 12 + 2 X 2.069 = 16.138 mm. The value of analytically determined diameter after 50% equals to 12 X $\sqrt{2}$ = 16.968 mm, (assuming volume constancy) leading to a very little error of 4.89% usually can be discarded in non-linear finite element analysis such as in large deformation / metal forming applications. Hence the analysis procedure adopted is validated. This fact was proved for all the alloys considered and hence, the homogeneous metal flow was found to be independent of material.

The development of barreling in the samples of AA2024 alloy and AA2024 alloy- 2 - 10 % fly ash composites was observed with friction. For the present study the friction factor 'm' was found to be 0.36 and the extent of barreling with this friction at 50% deformation for alloy and composites under investigation was shown in figures 700-5.40 respectively. These results were supported by many authors [12-27]. Lower aspect ratio (H_O/D_O = 1.0) samples has shows more barreling affect compare to higher aspect ratio (H_O/D_O = 1.5). The above results were experimentally evidenced.

The figures from 7 to 39 show the sample profiles of various quantities in global Cartesian co-ordinates for AA2024 alloy and AA2024 alloy- 2 - 10 % fly ash composites billet and tools in dry conditions with aspect ratios of 1.0 and 1.5 at the instance of 50% deformation viz., radial displacements (UX): circumferential stress, σ_θ (SY), axial stress σ_z (SZ), hydrostatic stress, σ_H (NLHPRE), Von-Mises equivalent stress $\overline{\sigma}$ (SEQV). The notations in the brackets were the default notations of Ansys FEA package.

These figures 7-39 were shown to compare the variation of stress components; circumferential, axial and hydrostatic stresses with the amount of fly ash content. The analysis was performed for the AA2024 alloy and AA2024 alloy- 2 - 10 % fly ash composites and the results of sub-grid quantities equivalent to the grid drawn on the sample during the upset test (chapter 4) were noted. For all the samples the circumferential stress and hydrostatic stress was maximum at the equatorial surface the specimen. But the axial stress was maximum at the mid height on the axis of specimen. With decrease in aspect ratio the hydrostatic stress increased at equatorial surface for all the alloy and composites under investigation.

The variations in FEA results compared to analytical results obtained in chapter 4 were shown in figures 5.41 to 5.44 for AA 2024 alloy and AA2024 alloy- 2 - 10 % fly ash composites respectively. The obtained FEA results revealed that these values are closely matching with the experimental values with a maximum deviation of less than 5%.

Fig-2 Un deformed sample (H_O/D_O = 1.0)

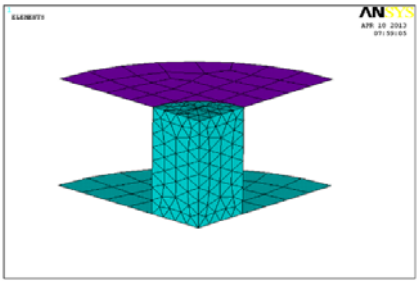

Fig 3: Un deformed sample (H_O/D_O = 1.5)

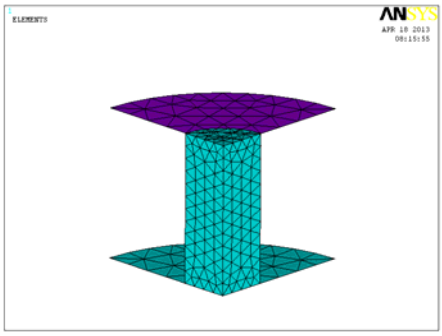

Fig 4: Deformed sample (H_O/D_O = 1.0) at 50% deformation for zero friction

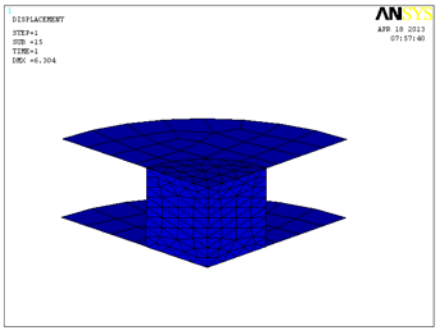

Fig 5: Deformed sample (H_O/D_O = 1.5) at 50% deformation for zero friction

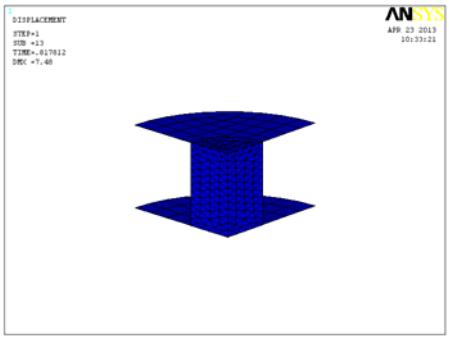

Fig 6: Radial displacement at 50 % deformation for zero friction (H_O/D_O = 1.0)

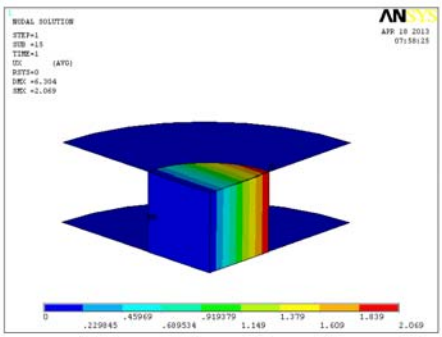

Fig 7: Radial displacement at 50 % deformation for zero friction (H_O/D_O = 1.5)

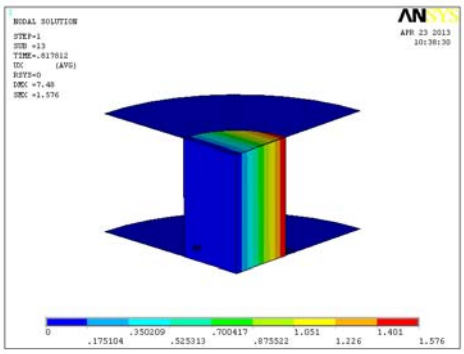

Fig 8: Circumferential Stress at 50% deformation of AA 2024 alloy (H_O/D_O= 1.0)

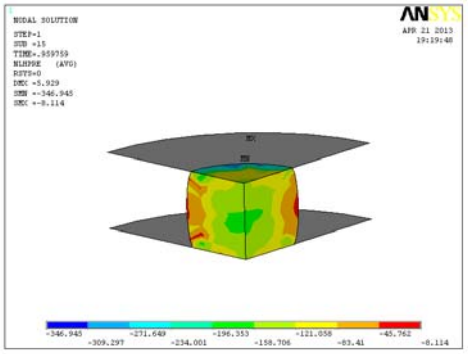

Fig 9: Circumferential Stress at 50% deformation of AA 2024 alloy (H_O/D_O=1.5)

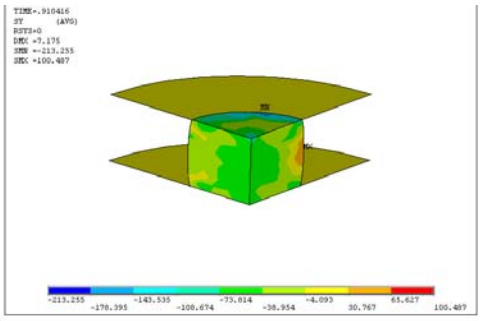

Fig 10: Axial Stress at 50% deformation of AA 2024 alloy (H_O/D_O= 1.0)

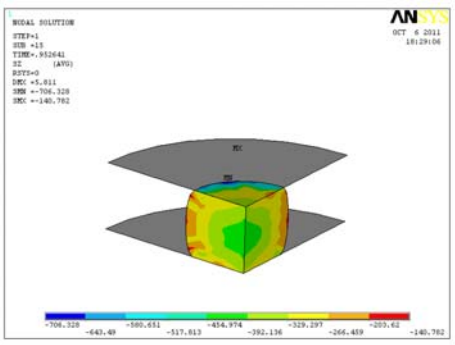

Fig 11: Axial Stress at 50% deformation of AA 2024 alloy (H_O/D_O= 1.5)

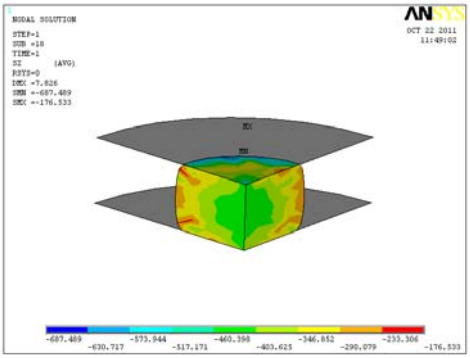

Fig 12: Hydrostatic Stress at 50% deformation of AA 2024 alloy (H_O/D_O= 1.0)

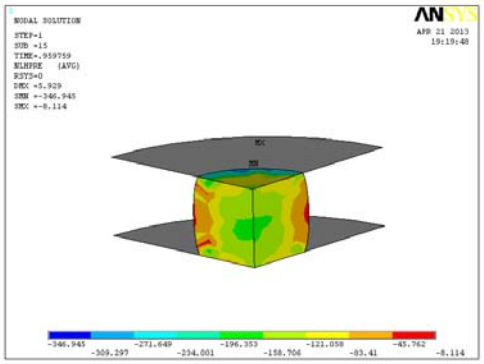

Fig 13: Hydrostatic Stress at 50% deformation of AA 2024 alloy (H_O/D_O= 1.5)

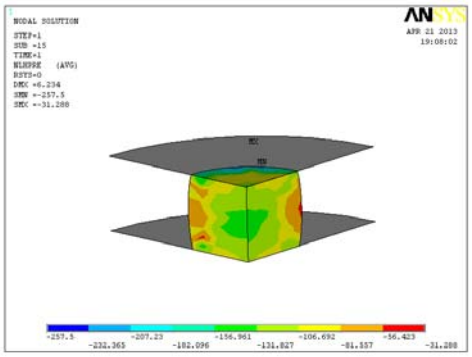

Fig14 : Von-Mises Stress at 50% deformation of AA 2024 alloy (H_O/D_O= 1.0)

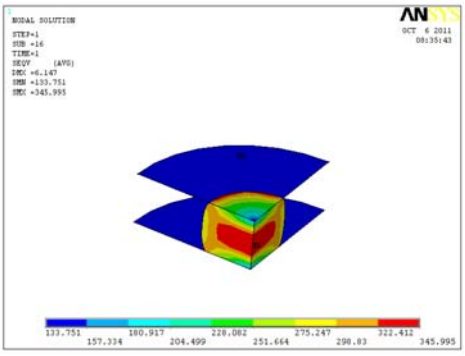

Fig 15: Von-Mises Stress at 50% deformation of AA 2024 alloy (H_O/D_O= 1.5)

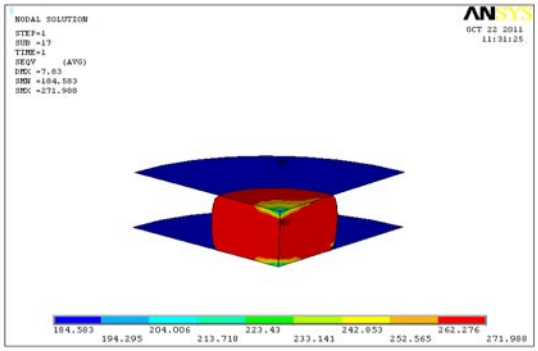

Fig 16: Circumferential Stress at 50% deformation of AA 2024 alloy-2% Fly Ash composite (H_O/D_O= 1.0)

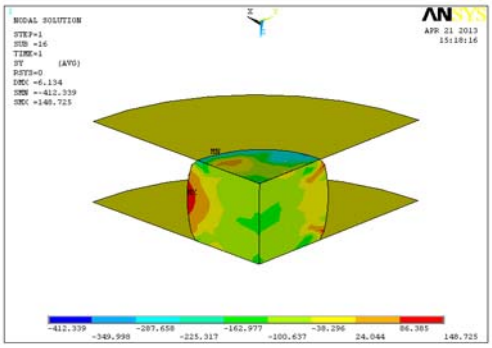

Fig 17: Circumferential Stress at 50% deformation of AA 2024 alloy-2% Fly Ash composite (H_O/D_O= 1.5)

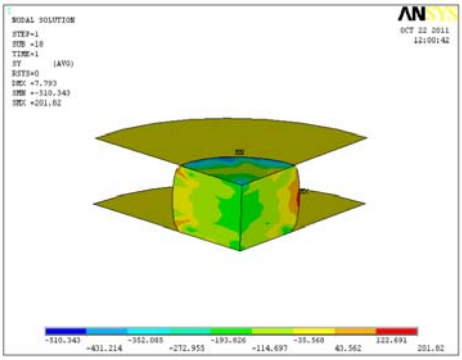

Fig 18: Axial Stress at 50% deformation of AA 2024 alloy-2% Fly Ash composite (H_O/D_O= 1.0)

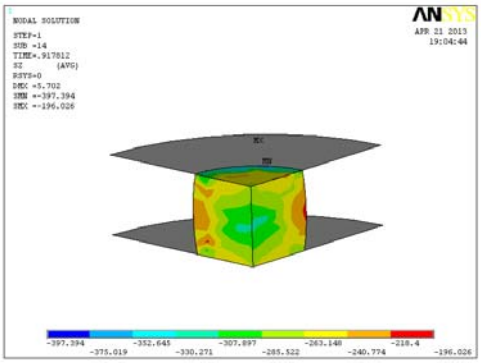

Fig 19: Axial Stress at 50% deformation of AA 2024 alloy-2% Fly Ash composite (H_O/D_O= 1.5)

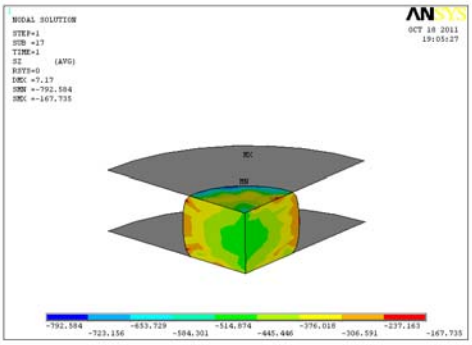

Fig 20 : Hydrostatic Stress at 50% deformation of AA 2024 alloy-2% Fly Ash composite (H_O/D_O= 1.0)

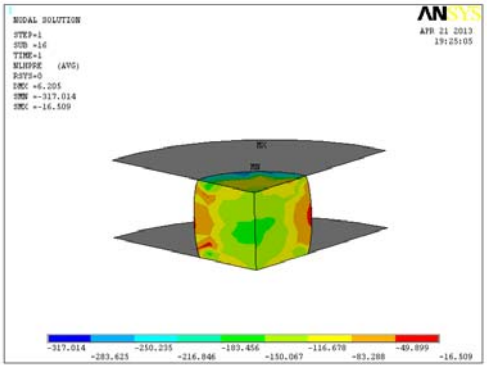

Fig 21: Hydrostatic Stress at 50% deformation of AA 2024 alloy-2% Fly Ash composite (H_O/D_O= 1.5)

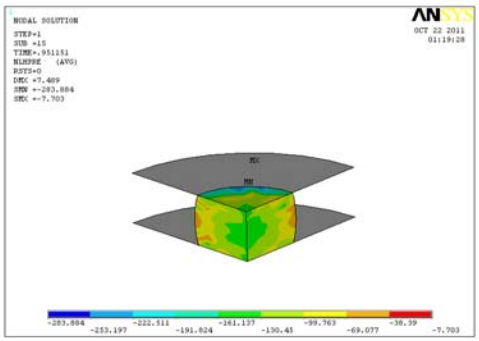

Fig 22: Von-Mises Stress at 50% deformation of AA 2024 alloy-2% Fly Ash composite (H_O/D_O= 1.0)

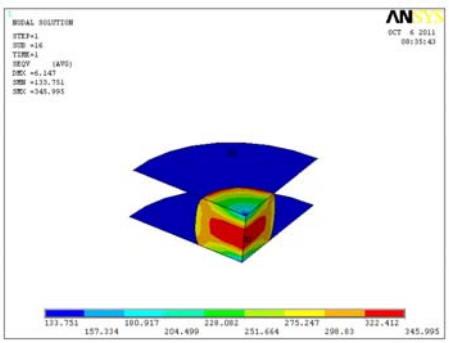

Fig 23: Von-Mises Stress at 50% deformation of AA 2024 alloy-2% Fly Ash composite (H_O/D_O= 1.5)

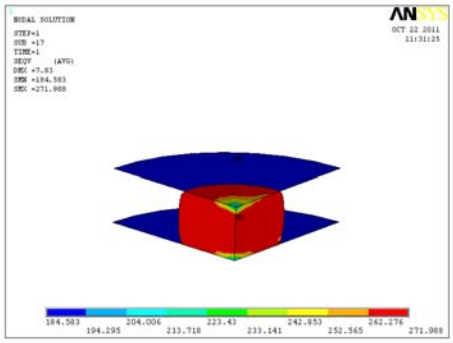

Fig 24: Circumferential Stress at 50% deformation of AA 2024 alloy-6% Fly Ash composite (H_O/D_O= 1.0)

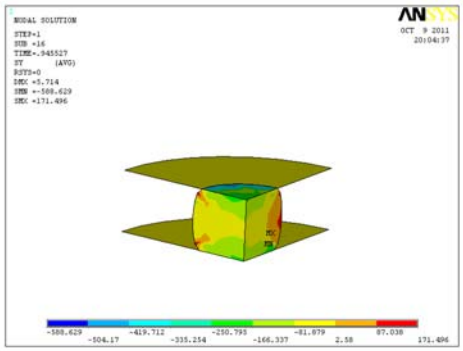

Fig 25: Circumferential Stress at 50% deformation of AA 2024 alloy-6% Fly Ash composite (H_O/D_O= 1.5)

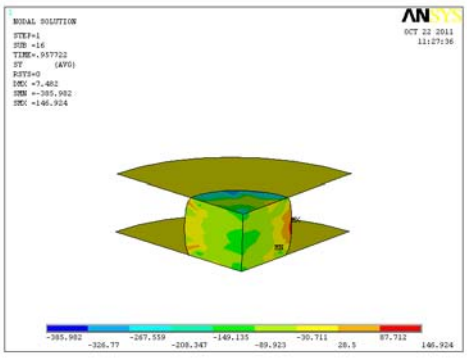

Fig 26: Axial Stress at 50% deformation of AA 2024 alloy-6% Fly Ash composite (H_O/D_O= 1.0)

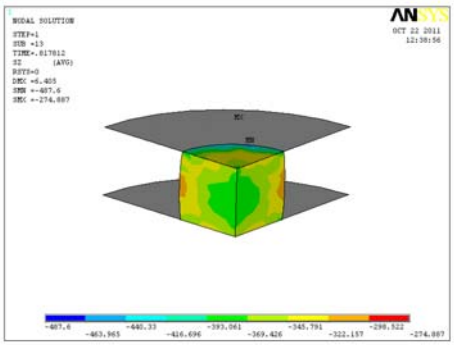

Fig 27: Axial Stress at 50% deformation of AA 2024 alloy-6% Fly Ash composite (H_O/D_O= 1.5)

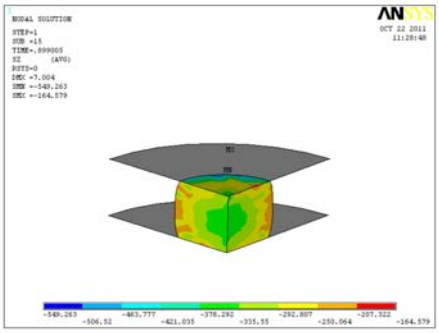

Fig 28: Hydrostatic Stress at 50% deformation of AA 2024 alloy-6% Fly Ash composite (H_O/D_O= 1.0)

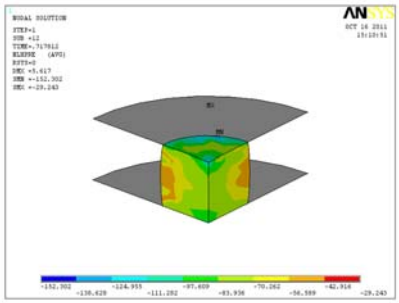

Fig 29: Hydrostatic Stress at 50% deformation of AA 2024 alloy-6% Fly Ash composite (H_O/D_O= 1.5)

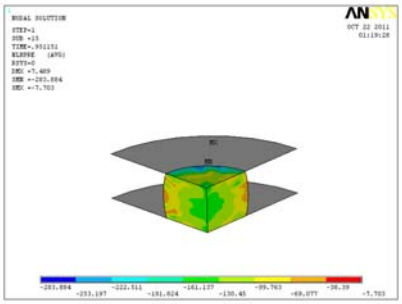

Fig 30: Von-Mises Stress at 50% deformation of AA 2024 alloy-6% Fly Ash composite (H_O/D_O= 1.0)

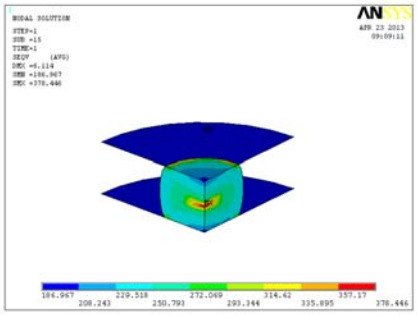

Fig 31: Von-Mises Stress at 50% deformation of AA 2024 alloy-6% Fly Ash composite (H_O/D_O= 1.5)

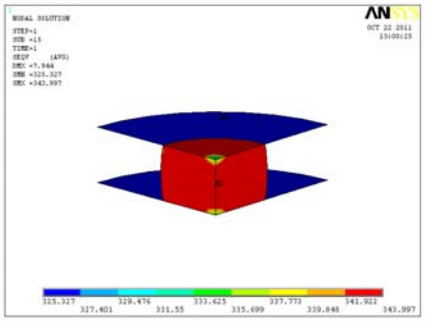

Fig 32: Circumferential Stress at 50% deformation of AA 2024 alloy-10% Fly Ash composite (H_O/D_O= 1.0)

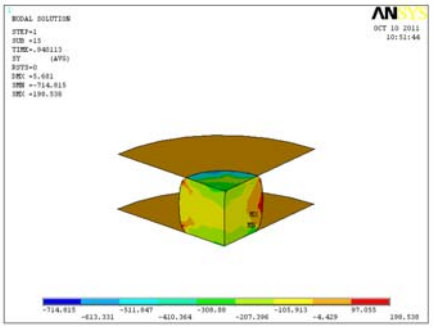

Fig 33: Circumferential Stress at 50% deformation of AA 2024 alloy-10% Fly Ash composite (H_O/D_O= 1.5)

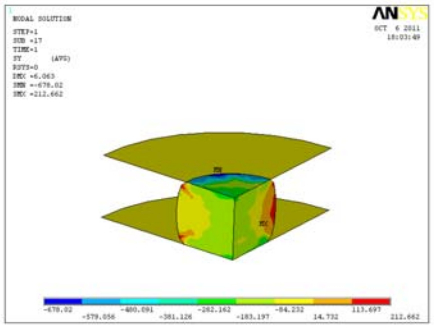

Fig 34: Axial Stress at 50% deformation of AA 2024 alloy-10% Fly Ash composite (H_O/D_O= 1.0)

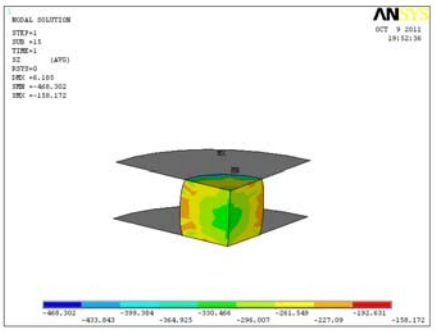

Fig 35: Axial Stress at 50% deformation of AA 2024 alloy-10% Fly Ash composite (H_O/D_O= 1.5)

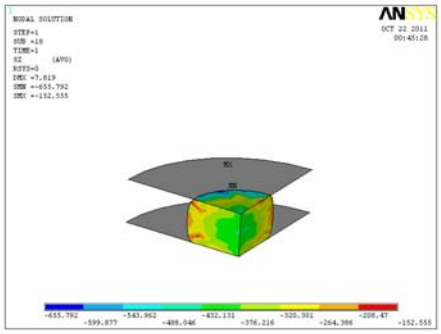

Fig 36: Hydrostatic Stress at 50% deformation of AA 2024 alloy-10% Fly Ash composite (H_O/D_O= 1.0)

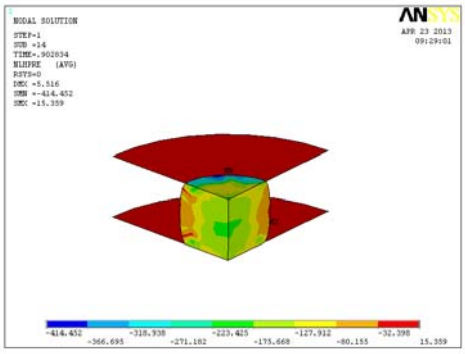

Fi g 37: Hydrostatic Stress at 50% deformation of AA 2024 alloy-10% Fly Ash composite (H_O/D_O= 1.5)

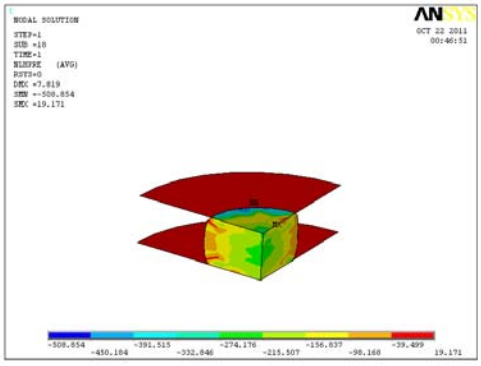

Fig 38: Von-Mises Stress at 50% deformation of AA 2024 alloy-10% Fly Ash composite (H_O/D_O= 1.0)

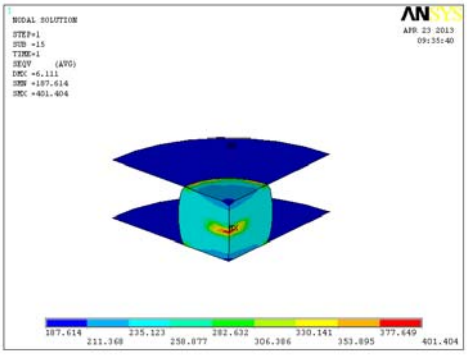

Fig 39: Von-Mises Stress at 50% deformation of AA 2024 alloy-10% Fly Ash composite (H_O/D_O= 1.5)

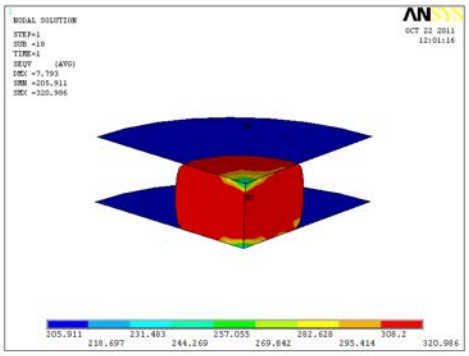

Fig 40: Comparative graphs between experimental and FEA values of Effective stress $\bar{\sigma}$, stress components σ_θ, σ_z and σ_H as a function of effective strain $\bar{\varepsilon}$ for AA2024 alloy; up to 50% deformed in dry condition with aspect ratio: (a) H_0/D_0 = 1.0, (b) H_0/D_0 = 1.5.

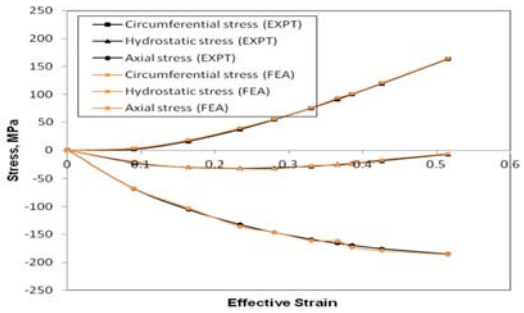

(a)

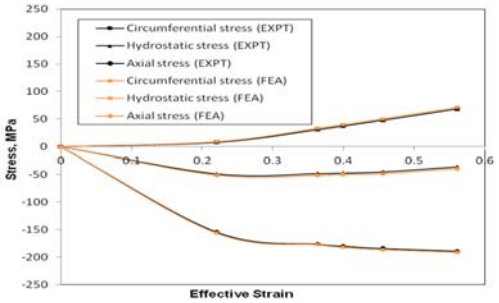

(b)

Fig 41: Comparative graphs between experimental and FEA values of Effective stress $\bar{\sigma}$, stress components σ_θ, σ_z and σ_H as a function of effective strain $\bar{\varepsilon}$ for AA2024 alloy-2% fly ash composite; up to 50% deformed in dry condition with aspect ratio: (a) H_0/D_0 = 1.0, (b) H_0/D_0 = 1.5.

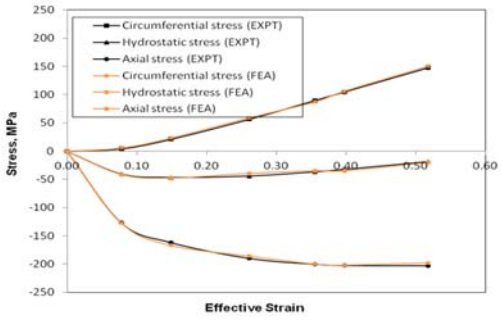

(a)

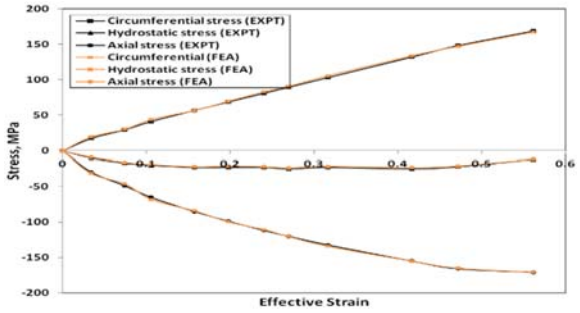

(b)

Fig 42: Comparative graphs between experimental and FEA values of Effective stress $\bar{\sigma}$, stress components σ_θ, σ_z and σ_H as a function of effective strain $\bar{\varepsilon}$ for AA2024 alloy-6% fly ash composite; up to 50% deformed in dry condition with aspect ratio: (a) H_0/D_0 = 1.0, (b) H_0/D_0 = 1.5.

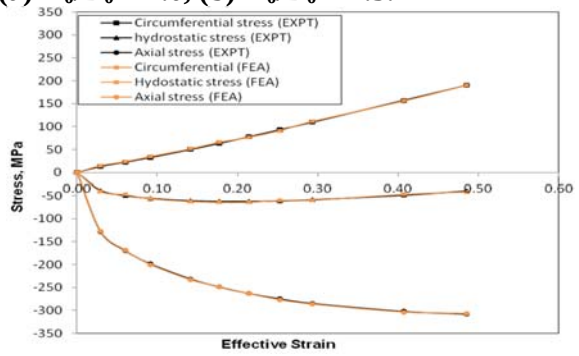

(a)

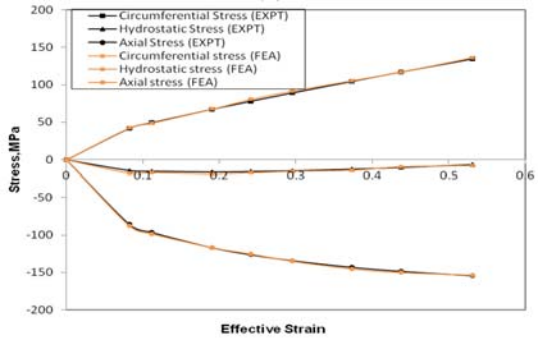

(b)

Fig 43: Comparative graphs between experimental and FEA values of Effective stress $\bar{\sigma}$, stress components σ_θ, σ_z and σ_H as a function of effective strain $\bar{\varepsilon}$ for AA2024 alloy-10% fly ash composite; up to 50% deformed in dry condition with aspect ratio: (a) H_0/D_0 = 1.0, (b) H_0/D_0 = 1.5.

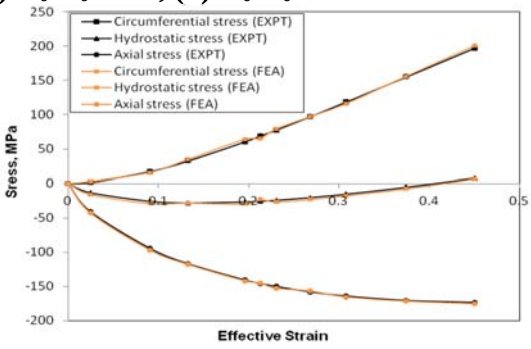

(a)

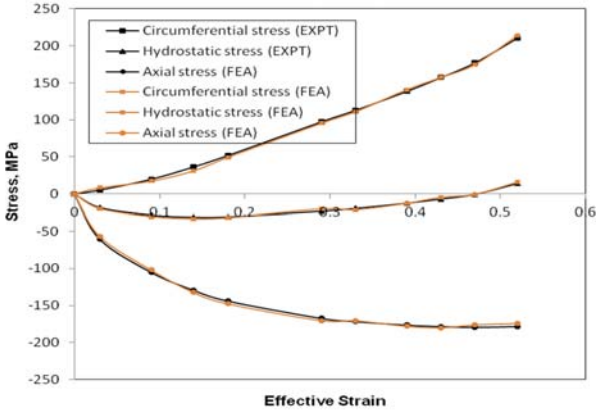

(b)

V. CONCLUSION

1. The cold upsetting process was modeled, simulated and analyzed with a sufficient accuracy.
2. The accuracy of results depends on the accuracy of the input data (true stress-true strain behaviour and friction factor obtained from the experiments) and friction model used in the analyses.
3. The time history data is useful in designing the intermediate dies for new materials.
4. The profile of the bulge during deformation can be estimated.
5. The analysis is useful in reducing the lead time of design cycle.
6. The machine down time can be reduced at production stage.

References

1. Singaresu S Rao., "The Finite Element method in Engineering", Elsevier Butterworth-Heinemann 2005 edition.

2. Kopp, R., Cao, M.L., de Souza, M.M., "Multi-level Simulation of Metal Forming Process", Proc. 2nd ITCP, Stuttgart, p.1128-1234, August, 1987.
3. ANSYS 10.0 Help manual documentation.
4. Wu, W.T., Jinn, J.T., and Fischer, C.E. "Modelling Techniques in Forming Processes" Scientific Forming Technologies Corporation. Chapter15. http://www.asminternational.org/Template.cfm?Section=BrowsebyFormat&template=Ecommerce/FileDisplay.cfm&file=06701G_ch.pdf
5. http://www.matweb.com
6. Lee C.H. and Kobayashi S., "New Solutions to Rigid-Plastic Deformation Problems Using a Matrix Method", J. Eng. Ind. (Trans. ASME), vol. 95, 1973, p 865
7. Oh, S. I., and Kobayashi S., "Workability of aluminium alloy 7075 T-6 in upsetting and rolling", Trans. ASME, J. Eng. Ind vol. 95, 1976, p 800-806.
8. Kobayashi, S., Oh, S.I., and Altan T., "Metal Forming and the Finite Element Method", Oxford University Press, New York, 1989
9. Zeinkiewiez O.C., "Flow Formulation for Numerical Solution of Forming Processes", in. PITTMAN J.F.T et al. (Eds), "Numerical Analysis of Forming Processes", Wiley. New York, 1984, pp 1- 44.
10. Jackson J.E., JR and Ramesh. M.S., "The Rigid-Plastic Finite Element Method for Simulation of Deformation Processing" in HARTLEY. P. et al. (Eds), "Numerical Modelling of Material Deformation Processes", Springer-Verlag, London, 1992, pp 148-177
11. Forging Modelling Project, School of Mechanical Engineering, University of Bath, Report FMP-3, 12-12-1994.,http://www.bath.ac.uk/mech-eng/fsu/fmppage/reports/fmp19/fmp19.pdf
12. http://www.matweb.com
13. Jolgaf, M., Hamouda, A.M.S., Sulaiman, S., Hamdan, M.M., "Development of a CAD/CAM system for the closed–die forging process", Journal of Material Processing Technology, vol 138, 2003, pp 436-442.
14. Taylan Altan and Dan Hannan "Prediction and Elimination of Defects in Cold Forging Using Process Simulation" R&D Update Forging, The Engineering Research Center for Net Shape Manufacturing, 2002, http://www.erensm.org
15. Bramley, A.N, and Mynors, D.J., "The use of forging tools" Materials and Design, vol 21, 2000, pp 279-286.
16. Weronski, W., Gontarz, A., and Pater, Zb., "The reason for structural defects arising in forgings of aluminium alloys analysed using the finite element method" Journal of Materials Processing Technology, vol 92-93, 1999, pp 50-53.
17. Kusiak,J., Pietrzyk,M., Chenot,L., "Die Shape Design and Evaluation of Microstructure Control in the Closed-die Axisymmetric Forging by Using FORGE2 Program" ISIJ International, vol 34, 1994, No 9, pp 755-760.
18. Chitkara,N.R., and Kim,Y, "Simulation of Upset Heading, Application of Rigid-Plastic Finite Element Analysis and some Experiments" The International Journal of Advanced Manufacturing Technology, vol 20, 2002, pp 589-597.
19. Lin, S.Y., "Investigation of Die-Workpiece Interface Friction with Lubrication During the Upsetting Process" The International Journal of Advanced Manufacturing Technology, vol 15, 1999, pp 666-673.
20. Oh, S.I., "Finite Element Analysis of Metal Forming Processes with arbitrarily Shaped Dies", International Journal of Mechanical Science, vol 24, No.8, 1982, pp 479-493.
21. Hoa, V.C., Seo, D.W., and Lim, J.K., "Site of ductile fracture initiation in cold forging: A finite element model", Theoretical and Applied Fracture Mechanics, vol 44, 2005, pp 58-69.